Surface Chemistry

DOI: 10.1002/ange.201206675

Improved Hydrothermal Stability of Mesoporous Oxides for Reactions in the Aqueous Phase**

*Hien N. Pham, Amanda E. Anderson, Robert L. Johnson, Klaus Schmidt-Rohr, and Abhaya K. Datye**

Catalysts for the production of biorenewable chemicals must operate under aqueous phase conditions, generally at temperatures above 473 K.[1,2] Conventional oxide supports designed for gas-phase reactions are not suitable for aqueous-phase reactions at these elevated temperatures. For example, alumina undergoes a phase change from γ-Al_2O_3 to boehmite at 473 K with a consequent loss of surface area.[3–5] Likewise, mesoporous silica SBA-15 suffers from collapse of the well-ordered mesoporous structure when heated to 473 K in liquid water, resulting in loss of its surface area and structural integrity.[6] In this work, we present a simple and inexpensive approach for modifying the surfaces of oxide supports to make them hydrothermally stable in liquid water at 473 K. This general approach can be applied to other oxides, but we report here the improvement in the hydrothermal stability of silica and alumina supports.

Our approach involves the deposition of a thin film of carbon (generally around 10 wt%) derived from simple sugars, such as sucrose. We demonstrate the utility of this approach through improved hydrothermal stability of SBA-15 mesoporous silica, commercial silica gel (Aldrich), and commercial fumed alumina (Degussa). Detailed procedures for catalyst synthesis are given in the Experimental Section. Hydrothermal treatment of each sample was carried out by heating it to 473 K at autogenous pressure (22 bar) and keeping this temperature for 12 hours.

Both alumina and silica gel have an open-pore structure, but SBA-15 has well-ordered cylindrical pores with a hexagonal structure. As we show here, the carbon coating can be successfully applied even to cylindrical pores with aspect ratios (length/diameter) that exceed 200. To confirm the presence of carbon on the pore walls of SBA-15, we acquired elemental carbon maps through energy-filtered transmission electron microscopy (EFTEM). Elemental-carbon maps of the SBA-15-based samples are shown in Figure 1, in which bright-red regions indicate the location of carbon in the EFTEM image at the carbon K edge. The uncoated SBA-15

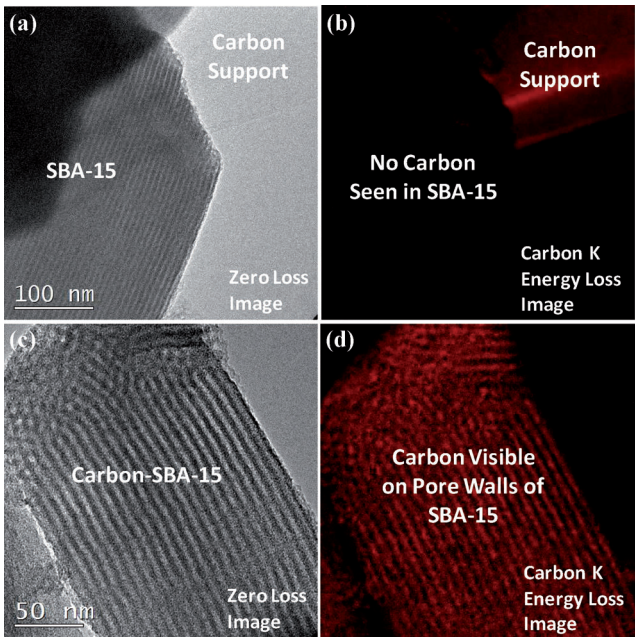

Figure 1. HRTEM images of calcined SBA-15 (a) and 10 wt% carbon-SBA-15 (c), and elemental carbon maps of SBA-15 (b) and 10 wt% carbon-SBA-15 (d).

particle is dark in the map (b), indicating that carbon is not present. For reference, the underlying carbon support film is visible in the EFTEM map in Figure 1b. The HRTEM image of carbon-coated SBA-15 (c) is similar to that of uncoated SBA-15 (a), because carbon does not produce any additional contrast in this image. However, the EFTEM image of coated SBA-15 (d) shows bright red regions showing the location of the carbon within the pores, and the dark regions within SBA-15 correspond to the silica walls. These images confirm that it is possible to coat the internal surfaces of the SBA-15 mesoporous silica with carbon. From the EFTEM image of coated SBA-15, it might appear that carbon has filled the pores of SBA-15. However, N_2 sorption isotherms obtained from the coated samples are very similar to the uncoated SBA-15, indicating a narrow pore-size distribution (see Figure S1 in the Supporting Information). Because of the coating, the pore diameter decreases from 4.8 nm in SBA-15 to 3.8 nm for carbon-coated SBA-15 (see Table S2). The major difference is the loss of microporosity and a decrease in

[*] Dr. H. N. Pham, A. E. Anderson, Prof. A. K. Datye
Department of Chemical & Nuclear Engineering
University of New Mexico, MSC 01 1120
Albuquerque, NM 87131-0001 (USA)
E-mail: datye@unm.edu
Homepage: http://www.unm.edu/~cmem
R. L. Johnson, Prof. K. Schmidt-Rohr
Department of Chemistry, Iowa State University
Ames, IA 50011 (USA)

[**] This work was supported by the Center for Biorenewable Chemicals supported by NSF grant EEC-0813570, and by the Partnership for International Research and Education supported by NSF grant OISE-0730277.

Supporting information for this article is available on the WWW under http://dx.doi.org/10.1002/anie.201206675.

total pore volume as a result of a narrowing of the pores. These are the major factors that cause a decrease in the total BET surface area of the carbon-coated sample.

HAADF-STEM images of the SBA-15-based samples (Figure 2) show the retained hexagonal arrangement of pores

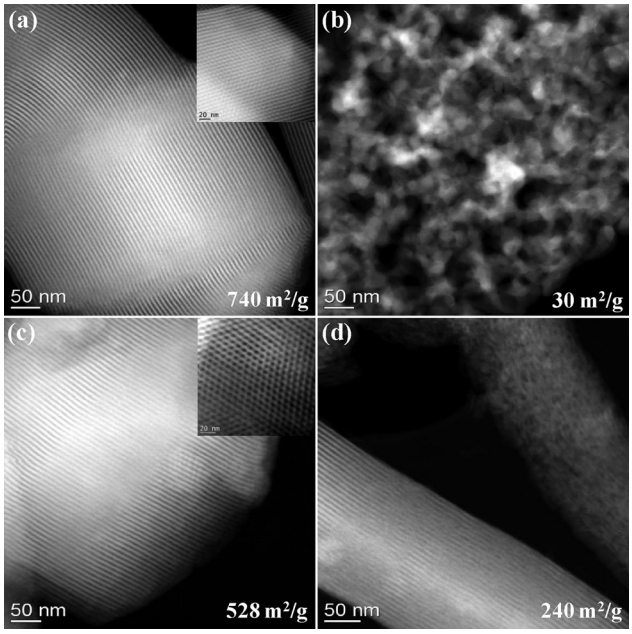

Figure 2. STEM images of calcined SBA-15 (a) and 10 wt% carbon-SBA-15 (c) with well-ordered hexagonal pores (insets), and of SBA-15 (b) and 10 wt% carbon-SBA-15 (d) after treatment in liquid water at 473 K for 12 h.

(inset) after coating the pore walls of SBA-15 (a) with carbon (c). After treatment in liquid water at 473 K for 12 hours, uncoated SBA-15 loses 96% of its surface area as a result of a complete collapse of the ordered mesopores, and loss of its structural integrity (Figure 2b). In contrast, hydrothermal stability is significantly improved after coating SBA-15 with carbon, with a surface-area loss of only 55% and a partially retained ordered mesoporous structure (d). If we increase the carbon loadings (e.g., 25 wt%), we can further retain the well-ordered structure of SBA-15 and minimize the loss of surface area after hydrothermal treatment (see Figure S3). For the silica gel based samples (Figure 3), uncoated silica gel (a) loses 75% of its surface area after hydrothermal treatment because of grain growth and sintering (b), whereas carbon-coated silica gel (c) neither loses surface area nor its structural integrity after hydrothermal treatment (d). For the alumina-based samples (Figure 4), uncoated alumina (a) loses 70% of its surface area after hydrothermal treatment (b), whereas both the morphology and surface area of carbon-coated alumina (c) are retained after hydrothermal treatment (d).

The chemical composition of the carbon layer was probed by solid-state NMR spectroscopy. Figure 5 shows the ^{13}C NMR spectrum of carbon-SBA-15 produced using ^{13}C-enriched glucose, with the corresponding spectrum of the nonprotonated carbon atoms (and mobile segments) superimposed. The spectra are dominated by signals of aromatic

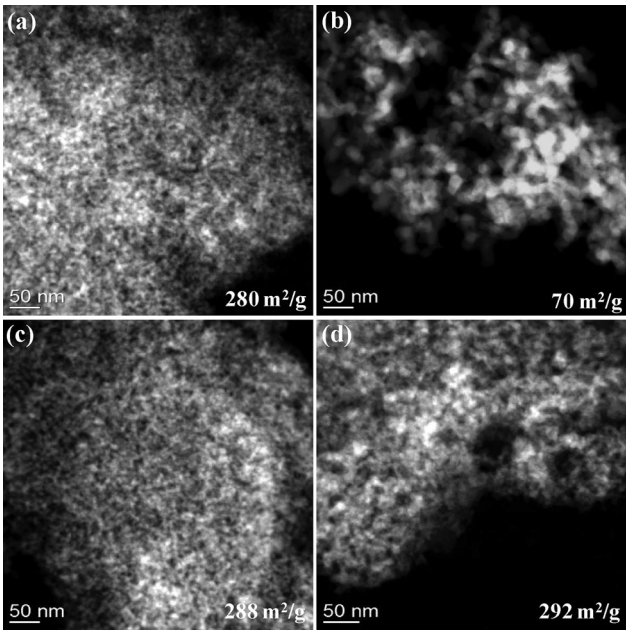

Figure 3. STEM images of silica gel (a) and 10 wt% carbon-silica gel (c), and of silica gel (b) and 10 wt% carbon-silica gel (d) after treatment in liquid water at 473 K for 12 h.

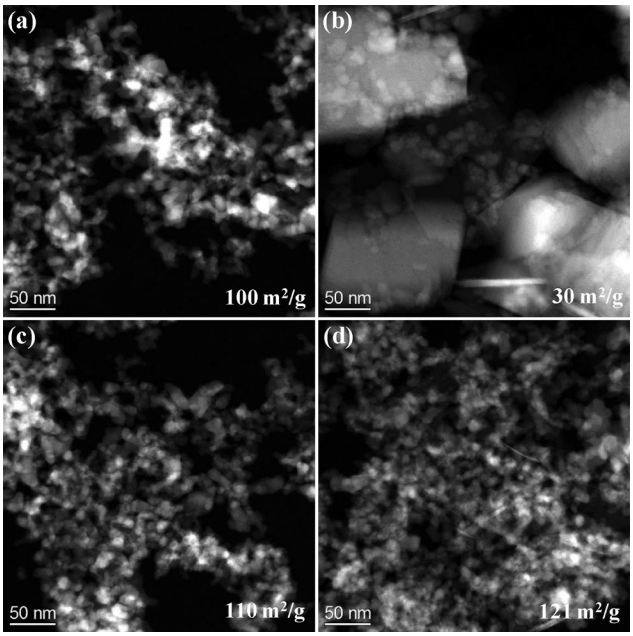

Figure 4. STEM images of fumed alumina (a) and 10 wt% carbon-alumina (c), and of fumed alumina (b) and 10 wt% carbon-alumina (d) after treatment in liquid water at 473 K for 12 h.

carbon atoms between 100 and 160 ppm (75% aromaticity). Nevertheless, CH_3 (3.5%), alkyl CH/CH_2 (5%), OCH_n (10%), COOH (3.5%), and C=O (3.5%) are also observed; a ^{13}C–^{13}C correlation NMR spectrum (see Figure S5) shows that the C=O and alkyl CH_n groups are attached to the aromatic rings, while many of the OCH_n carbon atoms are not. From the fractions of aromatic C–O (14%) and C–H (32%), and C=O, COO, and alkyl–C bonded to aromatic

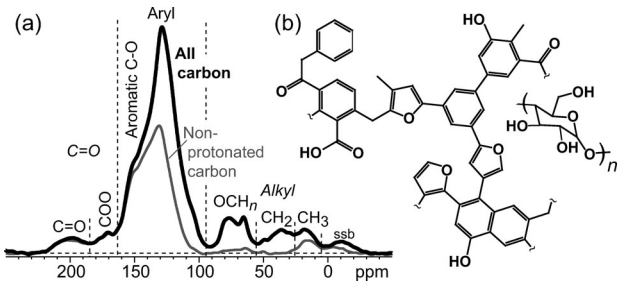

Figure 5. a) Quantitative ^{13}C NMR spectra of all carbon atoms (thick line), and of nonprotonated carbon atoms and CH_3 groups (thin line) in ^{13}C-enriched carbon-SBA-15, ssb = spinning sideband (14 kHz MAS); b) structural model reproducing the experimental spectra.

rings, one finds that aromatic carbon atoms that are bonded only to other aromatic carbon atoms, as found in polycondensed rings, account for approximately 1/5 of all signals of carbon atoms. Aromatic H–C–O intensity (see the Supporting Information) indicates that more than 6% of carbon atoms are part of furan rings. A structural model reproducing the measured spectra (see Figure S6) is shown in Figure 5b.

In addition to depositing a thin film of carbon on a concave surface, such as on the pore walls of SBA-15, we can improve the hydrothermal stability of oxides that have a convex surface, such as Stöber spheres, a nonporous silica with a BET surface area of 10 $m^2 g^{-1}$ (see Figure S7). After hydrothermal treatment, uncoated Stöber spheres show pronounced neck formation as a result of sintering of the spheres, as well as formation of large pores in the spheres. In contrast, hydrothermal stability is improved after coating Stöber spheres with carbon, with retention of the individual coated spheres and no pronounced sintering or formation of large pores after hydrothermal treatment. Furthermore, there is no delamination and formation of defects, which are generally more pronounced when thin films are deposited on convex surfaces rather than on concave ones.

The FTIR spectra of the SBA-15-based samples (see Figure S8) show a broad absorption band at around 3200–3600 cm,$^{-1}$ assigned to the O–H stretching vibration, and an absorption band at around 1640 cm,$^{-1}$ assigned to the bending vibrations of molecular water. Both the absorption bands at around 3200–3600 cm^{-1} and at around 1640 cm^{-1} are initially small for SBA-15, which is expected because FTIR was performed on SBA-15 just after calcination to remove the surfactant, thus minimizing exposure of SBA-15 to moisture. These two absorption bands slightly increased for carbon-coated SBA-15 after SBA-15 was mixed with the aqueous sucrose solution followed by carbonization. We then rehydrated each sample by resuspending it in water at room temperature overnight in order to determine the extent of re-adsorbed water on the pore walls of SBA-15. SBA-15 shows a significant increase in the absorption bands at around 3200–3600 cm^{-1} and at around 1640 cm^{-1} after rehydration, which indicates that water has re-adsorbed on the pore walls of SBA-15. In contrast, re-adsorption occurs to a much lesser extent for carbon-coated SBA-15. The results suggest that SBA-15 changes from a hydrophilic to a more hydrophobic state after coating the pore walls with 10 wt% carbon. The FTIR results are in agreement with improved hydrothermal stability for carbon-coated SBA-15. The surface of the uncoated silica samples used in this study consists of siloxane bridges and silanol groups. When silica is exposed to water at elevated temperatures, silicate hydrolysis occurs. The hydrolytic cleavage of the siloxane bonds leads to a dissolution and reprecipitation of silica, resulting in loss of both high surface area and structural integrity. By coating the surface of silica with carbon, we make the surface resistant to hydrolytic attack. With increased carbon loading, we are able to further improve the stability of the SBA-15 sample.

Figure 6 shows the XRD patterns of the alumina-based samples. Before hydrothermal treatment, the patterns for both uncoated (a) and carbon-coated alumina (b) are

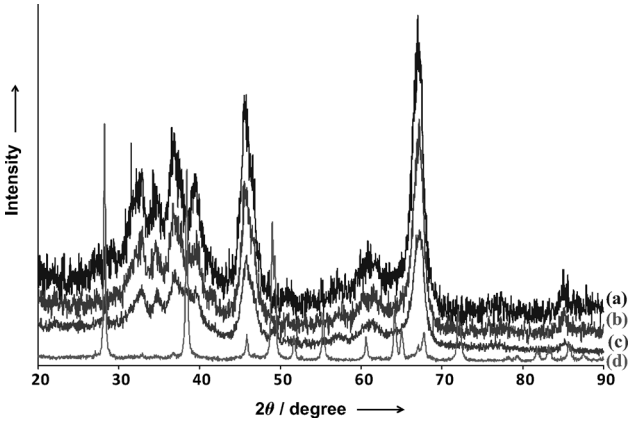

Figure 6. XRD patterns of fumed alumina (a) and 10 wt% carbon-alumina (b), and of 10 wt% carbon-alumina (c) and fumed alumina (d) after treatment in liquid water at 473 K for 12 h.

characteristic of the γ-Al_2O_3 phase. After hydrothermal treatment, the XRD pattern for uncoated alumina is characteristic of boehmite (d). The transformation from γ-Al_2O_3 to boehmite is due to hydration of alumina when it is subjected to liquid water at 473 K for several hours. In contrast, carbon-coated alumina remains as γ-Al_2O_3 after hydrothermal treatment (c). Similar changes in phase transformations were recently reported by Ravenelle et al.[3–5] In their work, they also found that the transformation of alumina to boehmite was inhibited when it was subjected to water in the presence of polyols, such as glycerol and sorbitol, at 498 K for several hours.[4] The increase in the hydrothermal stability of alumina was caused by the formation of carbonaceous layers which partially coated the surface of alumina, and therefore, prevented the transformation of γ-Al_2O_3 into boehmite. The extent of boehmite formation, however, depended on how well the carbonaceous species protected the alumina. In our work, we are able to modify the surface of alumina with carbon before subjecting it to hydrothermal conditions, thereby achieving improved stability. The extent of carbon coating, and the carbon loading, can be varied to achieve different degrees of surface modification of the γ-Al_2O_3 surface.

We have also explored the catalytic performance of carbon-coated oxides. The reaction we chose was the selective

hydrogenation of acetylene in the presence of excess ethylene. In previous work,[7] we found that Pd on carbon black was very selective toward ethylene while Pd on alumina was not selective. For this work, we compared the performance of 0.5 wt% Pd on the uncoated oxide with the corresponding oxide precoated with 10 wt% carbon. The catalysts contained similarly sized (1–1.5 nm) Pd nanoparticles (see Figure S9) prepared by direct alcohol reduction of Pd acetate at room temperature. A selective catalyst will convert all of the acetylene to ethylene without hydrogenating ethylene to ethane. However, as the acetylene conversion reaches 100%, all catalysts lose selectivity and start to show formation of ethane. The less-selective catalysts also hydrogenate some of the ethylene in the feed, thus leading to excess ethane. The amount of ethane formed is therefore a good measure of the selectivity of the catalyst, because selectivity at high acetylene conversion is desired. Ethane formation is presented as the ratio of moles of ethane in the effluent to moles of ethylene in the feed, which allows comparison with other feed compositions in the literature. The amount of ethane formed at the same acetylene conversion is high on the silica and alumina supports and lower on the carbon-coated supports (Figure 7),

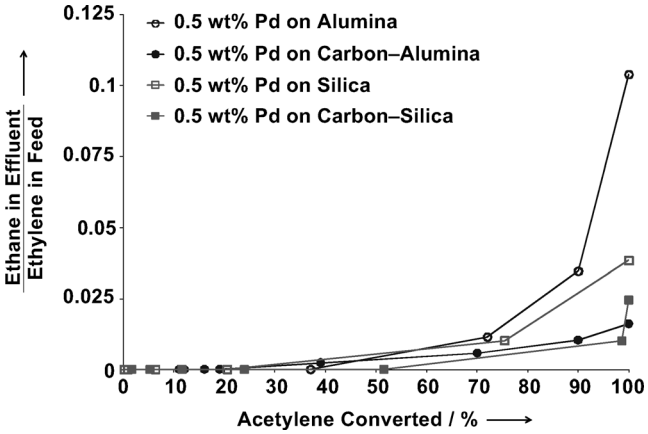

Figure 7. Selective hydrogenation of a mixture of acetylene/ethylene (1:70) on 0.5 wt% Pd on alumina (open circles) and on 10 wt% carbon-alumina (closed circles); 0.5 wt% Pd on silica gel (open squares) and on 10 wt% carbon-silica gel (closed squares).

which are comparable in selectivity to Pd/Vulcan XC carbon black. These catalysts prevent overhydrogenation of ethylene, even at near 100% conversion of acetylene. Addition of promoters, such as Ag, will further improve selectivity; here we use this test reaction to show changes in the surface chemistry at the metal–oxide interface. It is clear that coating these oxides with carbon changes the surface chemistry, making the surface more hydrophobic (fewer surface hydroxyls by FTIR); the oxide-surface chemistry is reflected in the improved selectivity for the acetylene hydrogenation. A hydrothermally stable support is necessary for achieving stable reactivity for metal-catalyzed reactions in the aqueous phase, as shown in our previous work.[6,8] Future work will explore the application of carbon-coated oxides for these reactions.

In conclusion, our results show that carbon coatings can impart improved hydrothermal stability to silica and alumina, which are otherwise not stable for aqueous-phase reactions. Thin-film coatings of carbon change the surface chemistry of the oxides, making them less susceptible to hydrolytic attack at elevated temperatures. We demonstrated that high dispersions of metal particles can also be achieved on these supports, opening up the possibility of novel catalyst designs that could be applied to demanding aqueous-phase reactions. The carbon coatings provide a simple route to create supports for biomass conversion with properties that conventional carbon supports may lack, such as mesoporosity and mechanical strength.

Experimental Section

To prepare mesoporous silica SBA-15, Pluronic P123 surfactant (4.0 g) was dissolved in deionized water (30 g) while stirring at 308 K. Once dissolved, 2 M HCl (120 g) and tetraethyl orthosilicate (TEOS; 8.6 g) were added to the solution. The solution was then transferred to a Nalgene bottle and placed in a water bath at 308 K without stirring for 20 h. The solid product was filtered, washed with deionized water, and air-dried at room temperature. The dried product was calcined in air at 773 K (5 K min^{-1} ramp) for 12 h to remove the P123 template.

To coat the surface of oxides with 10 wt% carbon, an aqueous solution of sucrose (^{13}C-glucose for NMR measurements) was added to SBA-15, silica gel, or fumed alumina. The mixture was stirred at room temperature overnight until the water evaporated. The dried product was collected and partially pyrolyzed under flowing UHP N_2 gas at 673 K (5 K min^{-1} ramp) for 2 h.

Palladium acetate was completely dissolved in methanol by sonication for 10 min, and the solution was added to the uncoated or 10 wt% carbon-coated oxides to obtain a Pd loading of 0.5 wt%. A Buchi rotary evaporator was used to gently remove methanol from the sample at 313 K, and the dried product was collected. Selective acetylene hydrogenation to ethylene was performed with a reactant mixture (0.5% acetylene, 35% ethylene, balance N_2; 70 cm^3 (STP) min^{-1}), hydrogen (3.5 cm^3 (STP) min^{-1}) and nitrogen (75 cm^3 (STP) min^{-1}), with a hydrogen/acetylene ratio of 7:1. Reactivity measurements for the samples (20 mg) were carried out at temperatures from 308 to 388 K, and the gas effluents were analyzed by GC (Varian CP-3800).

Samples were dispersed in ethanol and mounted on holey carbon grids for examination in a JEOL 2010F 200 kV transmission electron microscope. Images were recorded both in bright field (BF) and high-angle annular dark field (HAADF) modes. Elemental carbon maps were acquired using energy-filtered transmission electron microscopy (EFTEM) with an exposure time of 8 s for the SBA-15-based samples. Surface area was measured using N_2 adsorption at 77 K in a Micromeritics Gemini 2360 multipoint BET analyzer. N_2 sorption isotherms and pore-size distributions were measured at 77 K in a Quantachrome Autosorb-1 analyzer. Infrared spectra of samples were recorded on a Nicolet 7600 FTIR analyzer equipped with an attenuated total reflectance (ATR) attachment. The spectra were acquired between 400–4000 cm^{-1} at 4 cm^{-1} resolution and 128 scans. ^{13}C NMR spectroscopy was performed at 100 MHz on ^{13}C-enriched samples washed with water to remove trapped low-molar mass species, using a Bruker DSX400 spectrometer, magic-angle spinning at 14 kHz, and high-power ^{1}H decoupling. Quantitative ^{13}C NMR spectra were measured using direct polarization (DP) and a Hahn echo, with recycle delays of 30 s ($> 5\ T_1$), and spectra of nonprotonated carbon atoms (and mobile segments) were obtained after recoupled ^{13}C–^{1}H dipolar dephasing.[9] Details of the analysis of the spectra, also using spectral editing, are given in the Supporting Information. X-ray powder diffraction

(XRD) was performed using a Scintag Pad V diffractometer (Cu Kα radiation) with DataScan 4 software (MDI, Inc.).

Received: August 18, 2012
Revised: October 16, 2012
Published online: November 14, 2012

Keywords: aqueous phase · carbon · hydrogenation · hydrothermal stability · surface chemistry

[1] J. N. Chheda, G. H. Huber, J. A. Dumesic, *Angew. Chem.* **2007**, *119*, 7298 – 7318; *Angew. Chem. Int. Ed.* **2007**, *46*, 7164 – 7183.
[2] A. Corma, S. Iborra, A. Velty, *Chem. Rev.* **2007**, *107*, 2411 – 2502.
[3] R. M. Ravenelle, J. R. Copeland, W. G. Kim, J. C. Crittenden, C. Sievers, *ACS Catal.* **2011**, *1*, 552 – 561.
[4] R. M. Ravenelle, J. R. Copeland, A. H. Van Pelt, J. C. Crittenden, C. Sievers, *Top. Catal.* **2012**, *55*, 162 – 174.
[5] R. M. Ravenelle, F. Z. Diallo, J. C. Crittenden, C. Sievers, *ChemCatchem* **2012**, *4*, 492 – 494.
[6] Y. J. Pagán-Torres, J. M. R. Gallo, D. Wang, H. N. Pham, J. A. Libera, C. L. Marshall, J. W. Elam, A. K. Datye, J. A. Dumesic, *ACS Catal.* **2011**, *1*, 1234 – 1245.
[7] P. D. Burton, T. J. Boyle, A. K. Datye, *J. Catal.* **2011**, *280*, 145 – 149.
[8] H. N. Pham, Y. J. Pagan-Torres, J. C. Serrano-Ruiz, D. Wang, J. A. Dumesic, A. K. Datye, *Appl. Catal. A* **2011**, *397*, 153 – 162.
[9] J.-D. Mao, K. Schmidt-Rohr, *Environ. Sci. Technol.* **2004**, *38*, 2680 – 2684.

